Optics Letters

Broadband atomic-layer MoS_2 optical modulators for ultrafast pulse generations in the visible range

Yuxia Zhang,[1] Haohai Yu,[1,*] Rui Zhang,[1] Gang Zhao,[1] Huaijin Zhang,[1,4] Yanxue Chen,[2] Liangmo Mei,[2] Mauro Tonelli,[3] and Jiyang Wang[1]

[1]State Key Laboratory of Crystal Materials and Institute of Crystal Materials, Shandong University, Jinan 250100, China
[2]School of Physics, Shandong University, Jinan 250100, China
[3]NEST Istituto Nanoscienze-CNR and Dipartimento di Fisica dell'Università di Pisa, Largo B. Pontecorvo 3, 56127 Pisa, Italy
[4]e-mail: huaijinzhang@sdu.edu.cn
*Corresponding author: haohaiyu@sdu.edu.cn

Received 7 December 2016; revised 28 December 2016; accepted 2 January 2017; posted 5 January 2017 (Doc. ID 282101); published 27 January 2017

Visible lasers are a fascinating regime, and their significance is illustrated by the 2014 Noble prizes in physics and chemistry. With the development of blue laser diodes (LDs), the LD-pumped solid-state visible lasers become a burgeoning direction today. Constrained by the scarce visible optical modulators, the solid-state ultrafast visible lasers are rarely realized. Based on the bandgap structure and optoelectronic properties of atomic-layer MoS_2, it can be proposed that MoS_2 has the potential as a visible optical modulator. Here, by originally revealing layer-dependent nonlinear absorption of the atomic-layer MoS_2 in the visible range, broadband atomic-layer MoS_2 optical modulators for the visible ultrafast pulse generation are developed and selected based on the proposed design criteria for novel two-dimensional (2D) optical modulators. By applying the selected MoS_2 optical modulators in the solid-state praseodymium lasers, broadband mode-locked ultrafast lasers from 522 to 639 nm are originally realized. We believe that this Letter should promote the development of visible ultrafast photonics and further applications of 2D optoelectronic materials.

OCIS codes: (140.3480) Lasers, diode-pumped; (140.7300) Visible lasers; (140.7090) Ultrafast lasers; (160.4330) Nonlinear optical materials; (250.4110) Modulators.

https://doi.org/10.1364/OL.42.000547

Since the invention of lasers half a century ago, visible lasers have been considered as a significant and fascinating regime owing to the fact that they have wide applications and requirements in various topical ranges, including medicine, biomedical images, microscopy, scientific research, and our daily life [1,2]. Boosted by the development of blue LDs, 2014 Noble prizes in physics [3], solid-state visible lasers burgeon with the blue LDs as the pump sources and praseodymium (Pr^{3+})-doped crystals as the gain materials, and the continuous-wave (cw) operation has been power scaled to watt levels with high efficiency up to now [4]. However, limited by the rarity of practical optical modulators in visible ranges, ultrafast visible pulsed lasers, i.e., cw mode-locked lasers, are still under development, and only a semiconductor saturable absorber mirror (SESAM) based on well-designed GaInP quantum wells is available at the special application wavelength of 639 nm [5,6]. The discovery of optical modulators applied in the visible range is required.

From the discovery of the first graphene optical modulator [7], two dimensional (2D) materials have been widely studied and considered as the promising optical modulators in ultrafast photonics due to their high-carrier mobility, picosecond or femtosecond photo-generated carrier lifetime, and high optical absorption coefficient [8,9]. Up to now, few of them have been employed in solid-state visible lasers [10,11] which constrained their applications in the visible photonics. Based on the basic ultrafast laser theory and current investigation situation of 2D semiconductors [9,12], 2D optical modulators for the ultrafast visible lasers must have a bandgap less than 1.7 eV corresponding to 700 nm and a short photocarrier recombination time that should be shorter than the laser cavity round-trip time T_R of about 10 ns [13]. Atomic-layer transition-metal dichalcogenides emerged and have shown amazing optoelectronic properties with sensitive photoresponse and saturable absorption [14]. The bandgaps of the monolayer MoS_2 and bulk MoS_2 have the value of 1.89 and 1 eV corresponding to the wavelength of 660 nm and near infrared wavelengths, respectively [15]. In recent years, MoS_2 has been used in passive Q-switching and mode locking as the optical modulator in the infrared range at the wavelengths from 1 to 2 μm [16,17] by using its metallic states [16] or by the introduction of suitable defects [14], strain engineering [18], vertical electric field [19], etc. MoS_2 should also be an excellent optical modulator in the visible range, whether in the monolayer or bulk [20]. Here, by measuring the layer-dependent nonlinear absorption of MoS_2, the appropriately layered broadband MoS_2 optical modulators were selected for the first time, to the best of our knowledge, and primarily applied in the mode-locked Pr^{3+} visible lasers with wavelengths from 522 to 639 nm.

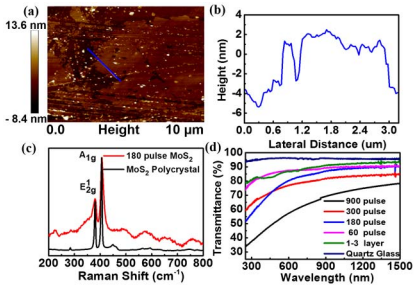

Fig. 1. (a) Morphology of a 13-layer MoS_2 sample measured with the AFM, (b) typical variation of a MoS_2 sample height, (c) Raman spectra of 13-layer MoS_2 sample and polycrystalline MoS_2, and (d) transmission spectra of a prepared MoS_2/quartz glass sample and quartz glass substrate.

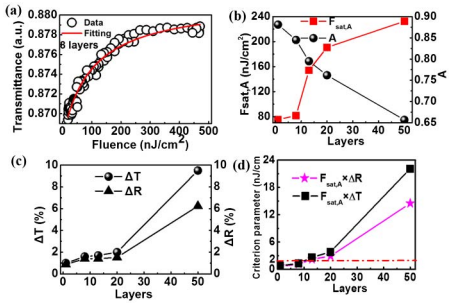

Fig. 2. (a) Result of transmittance and input fluence based on the eight-layer MoS_2 sample (inset: the layer-dependent saturable photo-induced electron-hole density N_s), (b) the relation between A, $F_{\mathrm{sat},A}$ and layers of prepared MoS_2 samples, (c) ΔT and ΔR with the change of layers, and (d) $F_{\mathrm{sat},A} \times \Delta R$ and $F_{\mathrm{sat},A} \times \Delta T$ with the change of layers.

Multilayer and 1–3-layer MoS_2 samples were produced by a pulsed laser deposition method and "chemical weathering" exfoliation with the commercial optical-grade far-ultraviolet quartz glass wafer as the substrates, respectively [14,20,21]. The layers and morphology of the prepared MoS_2 samples were characterized with the atomic force microscopy (AFM). It showed that the prepared samples have a thickness of 30 to 0.6 nm corresponding to the layers of about 50, 20, 13, 8, and 1–3 [22]; the AFM results of 13-layer MoS_2 sample are presented in Figs. 1(a) and 1(b) as a representative. The vibration modes of all the samples were studied with the results that the in-plane E^1_{2g} and out-of-plane A_{1g} vibrational appeared at 378 and 400 cm^{-1}. The vibration modes of 13-layer samples are shown in Fig. 1(c). In comparison with the Raman spectrometer of polycrystalline MoS_2, the A_{1g} mode was a little red-shifted which matched well with the previous Letter [23]. The transmission spectra of these five prepared MoS_2 samples and the quartz glass wafer substrate were also measured from 250 to 1500 nm with the UV/VIS/NIR spectrophotometer (*V-570 JASCO*) and are shown in Fig. 1(d). As can be seen in this figure, the transmission of all samples increased with the increase of the wavelengths, and the increasing speeds were distinctly different.

To explore the relationship between nonlinear absorption and layers, 50, 20, 13, 8, and 1–3-layer MoS_2 samples were characterized by the Z-scan technique, and a detailed experimental setup was described in our other Letter [13]. In theory, the fluence-dependent transmission can be shown in the form as in [24]:

$$T(F) = \exp(-\alpha d) = A \exp\left(-\frac{\Delta T}{1 + \frac{F}{F_{\mathrm{sat},A}}}\right), \quad (1)$$

where F is the irradiation fluence, $F_{\mathrm{sat},A}$ is the saturable irradiation fluence, d is the thickness of the sample, $A = \exp(-\alpha_{NS} d)$ is the unsaturable absorption, and $\Delta T = \alpha_S d$ is the normalized modulation depth. The modulation depth ΔR which indicates the difference between the finial and initial transmission can be expressed as

$$\Delta R = T(F \to \infty) - T(F \to 0) \approx A \Delta T. \quad (2)$$

Fitted by Eq. (2), the typical nonlinear optical absorption with the fluence-dependent transmittance of all samples measured by the Z-scan technique were achieved and demonstrated in Fig. 2(a) with the eight-layer MoS_2 sample as the example. The resulting saturable fluence $F_{\mathrm{sat},A}$, unsaturable absorption A, and normalized modulation depth ΔT are shown in Figs. 2(b) and 2(c), respectively. As shown in the two figures, both $F_{\mathrm{sat},A}$ and ΔT increased with the layers, which could be understood by the saturable photocarrier density corresponding to the available sates for the photocarriers. The variation of A showed that the scatterings or defects for the prepared samples decreased with the layers, which indicated the perfection of samples, especially for the multilayers. Based on the measured saturable fluence and the reported carrier recombination time of MoS_2 samples [25], the layer-dependent saturable photo-induced electron-hole density N_s was calculated, as shown in the inset of Fig. 2(a), which indicated that the available states for the photocarrier corresponding to the effective volume increase with the layers of the samples. The decreased A and increased ΔT determined the variation of ΔR with the layers, as shown in Fig. 2(c).

During the ultrafast photonics applications, the nonlinear saturable absorption of optical modulators is related to the Q-switched mode-locked (QML) instability status which is the obstacle in cw mode-locked lasers [26]. According to the [27], the relationship between laser dynamics and saturable absorption can be derived and expressed as

$$F_{\mathrm{sat},A} \Delta R < \frac{(PT_R)^2}{F_{\mathrm{sat},L} \times A_{\mathrm{eff},L} \times A_{\mathrm{eff},A}} = \frac{(PT_R)^2 \times m\sigma_L \lambda}{hc \times \pi\omega^2_{\mathrm{eff},L} \times \pi\omega^2_{\mathrm{eff},A}}, \quad (3)$$

where $E_p = P \times T_R$ with the average intracavity laser power P. $E_{\mathrm{sat},X} = F_{\mathrm{sat},X} \times A_{\mathrm{eff},X}$ is the saturation energy of the laser gain material ($X = L$) and saturable absorber ($X = A$) with the saturation fluence $F_{\mathrm{sat},X}$ and the effective laser mode areas $A_{\mathrm{eff},X}$, respectively. $F_{\mathrm{sat},L} = h\nu/m\sigma_L$ and h is a Planck constant; ν is the photon frequency, m is a constant, and σ_L is the emission cross section of the laser gain material. For a ring cavity, $m = 1$ while, for a simple standing wave cavity, $m = 2$. $A_{\mathrm{eff},X} = \pi\omega_{\mathrm{eff},X^2}$, with the effective radius $\omega_{\mathrm{eff},X}$ of the laser mode. In this equation, the left-hand side is the unique nonlinear optical absorption properties of saturable absorber, including the saturation fluence $F_{\mathrm{sat},L}$ and modulation depth ΔR; meanwhile,

the right-hand side is the parameters about the laser gain material and laser cavity.

For blue LD-pumped visible mode-locked lasers, the emission cross section σL of the laser gain material is in the magnitude of 10–20 cm^2 [4], and the laser cavity length is generally selected as about 1.5 m with TR of 10 ns [5,28]. The available pump beam radius in the gain material is about 50 μm, and the laser beam radius on the saturable absorber is about 30 μm. With the low limit for the mode locking, the intracavity power is about 1 W, e.g., the output coupler transmittance of 0.1% and stable cw mode-locking threshold of 1 mW. Then, the right-hand side of Eq. (3) can be calculated as 1.6 to 2 nJ/cm^2 for the visible laser at the wavelengths from green (about 520 nm) to deep red (about 720 nm). This implies that if we want to obtain a mode-locked visible laser with a relatively low threshold, the left-hand side parameter ($F_{sat,A} \times \Delta R$) of the 2D optical modulators should be less than 2 nJ/cm^2 orders of magnitude, which indicates that both the modulation depth ΔR and saturation fluence $F_{sat,A}$ of the 2D optical modulators influence the mode-locking performance, and the large modulation depth corresponds to low saturation fluence or instead. It should be noted that for femtosecond soliton lasers, some other specific parameters were needed, but the emission spectral width (about 1 nm) of the active ions confines the achievement of this condition [27].

The critical nonlinear absorption parameters ($F_{sat,A} \times \Delta R$) and ($F_{sat,A} \times \Delta T$) were calculated and are shown in Fig. 2(d), which represent the selection criteria for the present prepared samples and ideal samples without unsaturable absorption. From Fig. 2(d), it can be found that the present 13-layer sample with $F_{sat,A} \times R = 2.2$ nJ/cm^2 is near the critical lines $F_{sat,A} \times \Delta R = 2$ nJ/cm^2, but the critical parameter ($F_{sat,A} \times \Delta T$) of the 13-layer sample becomes far from the critical line. In consideration of the estimation in the theoretical basis, $F_{sat,A} \times \Delta R$ of eight- and 1–3 layer MoS_2 samples are in the magnitude of 1 nJ/cm^2, and both of the MoS_2 samples should be the most appropriate optical modulators in Pr^{3+} ion—doped fluoride crystal visible mode-locked lasers.

In the visible mode-locked laser design, the experimental setup is shown in Fig. 3. A 1.01 at. % *a*-cut Pr^{3+}:$GdLiF_4$ crystal has been chosen as the gain material with dimensions of 2.7 × 3.2 × 6.9 mm ($a \times c \times a$). The crystal's end surfaces were polished and antireflection coated at the wavelengths of 440–450 nm and 500–750 nm. The pump source was a 3.5 W blue LD with the wavelength of 444 nm. With a focusing system composed of two lens (f1 = f2 = 100 mm), the laser beam radius in Pr^{3+}:$GdLiF_4$ crystal $A_{eff,L}$ was determined to be about 65 μm. The folded mirrors M1, M2, M3, and M4 were concave mirrors with the same curvature radii of 100 mm and the same coated parameters of high transmission at the wavelengths of 440–450 nm and high reflections at the wavelengths of 500–780 nm. The output coupler M5 was a plane mirror with different coated parameters for different output wavelengths. The MoS_2 optical modulator was installed at the beam waist place formed by M3 and M4 with its Brewster angle. Based on the ABCD matrix, the waist radii of the laser beam in a Pr^{3+}:$GdLiF_4$ crystal and in a MoS_2 optical modulator were calculated to be about 65 and 20 μm. By changing the output coupler M5, green (522 nm), orange (607 nm), and red (639 nm) mode-locked pulse lasers were obtained, respectively. The transmittance T_{OC} of M5 was 2%, 2%, and 1.8% at the wavelength of 522 nm, 607 nm, and 720 nm, respectively. The mode-locked pulses were recorded by the digital oscilloscope (*Tektronix MSO 72504DX*, 25 GHz bandwidth and 16 ps rise time) with an InGaAs photodetector (*New focus 1414*, 14 ps rise time). The laser spectra were displayed by the spectrometer (*YOKOGAWA AQ6315*, 0.05 nm resolution).

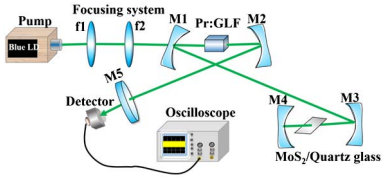

Fig. 3. Setup of the visible mode-locked laser.

The stable cw mode-locking pulse lasers at the wavelengths of 522, 607, and 639 nm were obtained with the eight- and 1–3-layer MoS_2 samples. The details of a 522 nm mode-locked laser with an eight-layer sample as the optical modulator are shown in Fig. 4. The relation of the average output power versus the absorbed pump power was achieved, as shown in Fig. 4(a), and a QML instability appeared when the absorbed pump power was less than 1.17 W with an average output power of 7 mW, which was consistent with the theoretical prediction. QML was suppressed gradually with the increase of the pump power, and stable cw mode locking was obtained. The maximum average output power was about 10 mW at an absorbed pump power of 1.3 W, and no optical damage was observed on the surfaces of the MoS_2 optical modulator which indicates that the optical damage threshold should be much larger than the present intensity 8 MW/cm^2. During the visible pulse experiment, the mode-locked pulses were monitored for an hour and the mode-locking is kept stable. Examples of stable cw mode-locked pulse trains are shown in Fig. 4(b) in 10 ns/div and 100 μs/div (inset) which indicates that the QML was fully suppressed. Single pulses were also recorded and are shown in Fig. 4(c) with a pulse width of 46 ps. The laser cavity length was optimized to be about 1.48 m which agreed well with the radio frequency (RF) spectra exhibited in Fig. 4(d) with the repetition rate of 101.4 MHz. The signal-to-noise ratio was about 55 dB above the background, and no QML instability was observed. With a spectrometer, the stable

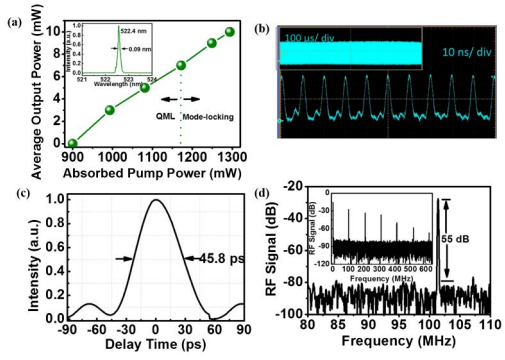

Fig. 4. (a) Average output power versus absorbed pump power at 522 nm (inset: the mode-locked spectrum of 522 nm), (b) pulse train recorded in 10 ns/div (inset: in 100 μs/div), (c) a single pulse trace, and (d) an RF spectrum with a frequency of 101 MHz (inset: a 600 MHz wide-span RF spectrum).

Table 1. Mode-Locked Experimental Data of 522, 607, and 639 nm

Wavelength (nm)	522.4	607.6	639.2	639 (1–3 layers)
Output Power (mW)	10	18	22	46
Repetition Rate (MHz)	101.4	90.2	104.4	94.7
Pulse Width (ps)	46	30	55	25
RF (dB)	55	58	64	77
FWHM (nm)	0.09	0.16	0.20	0.20

cw mode-locked spectrum was also measured and is shown in the inset of Fig. 4(a) with the center wavelength of 522.4 nm and the corresponding full width at half-maximum (FWHM) was about 0.09 nm. The passively mode-locked lasers at the wavelengths of 607 and 639 nm were also obtained and are listed in Table 1. With a 1–3-layer MoS_2 sample as the optical modulator, the laser performance at 639 nm was also obtained and is shown in Table 1. With a 1–3-layer MoS_2 sample, the stable cw mode locking was obtained at a relatively lower absorbed pump power (0.71 W) with a much higher average output power (46 mW). In addition, the pulse width was about 25 ps which is much narrower than that of an eight-layer MoS_2 sample experiment at the wavelength of 639 nm (55 ps) with a higher signal-to-noise ratio (77 dB) and higher intracavity power which may be associated with the accompanying Kerr effect. However, with the 13-layer MoS_2 sample and more layered MoS_2 samples, QML instabilities will suppress the achievement of cw mode locking.

In conclusion, based on the investigation of their layer-dependent nonlinear absorption properties of MoS_2 modulators, the ultrafast visible lasers with the wavelengths of 522, 607, and 639 nm were achieved with the pulse width of dozens of picosecond and the repetition rate of 100 million hertz. The experimental results were analyzed by the proposed design criteria of 2D optical modulators for the ultrafast mode-locked visible lasers. We found that critical nonlinear absorption parameters of $F_{\mathrm{sat},A} \times \Delta R$ of the MoS_2 less than 2 $\mathrm{nJ/cm^2}$ are suitable for the applications in the ultrafast mode-locked lasers. The present mode-locked laser results show some advantages in the aspect of output power over that achieved with the unique well-designed GaInP quantum well SESAM [5]. Meanwhile, MoS_2 has the advantages of being broadband, having easy preparation, and being low in cost. Besides providing novel ultrafast optical modulators in the visible range, we believe the design criterion should be helpful for the development of ultrafast photonics, especially in the burgeoning visible range, e.g., the generation of irradiation visible ultrafast source for the photo-activated localization microscopy.

Funding. National Key Research and Development Program of China (2016YFB0701002); Natural Science Foundation for Distinguished Young Scholars of Shandong Province (JQ201415); National Natural Science Foundation of China (NSFC) (51272131, 51372139, 51422205); Taishan Scholar Foundation of Shandong Province, China.

REFERENCES

1. R. G. Wheeland, Laser Surg. Med. **16**, 2 (1995).
2. J.-A. Conchello and J. W. Lichtman, Nat. Methods **2**, 920 (2005).
3. The Nobel Prize in Chemistry 2014, http://www.nobelprize.org/nobel_prizes/chemistry/laureates/2014/.
4. C. Kränkel, D. T. Marzahl, F. Moglia, G. Huber, and P. W. Metz, Laser Photon. Rev. **10**, 548 (2016).
5. M. Gaponenko, P. W. Metz, A. Härkönen, A. Heuer, T. Leinonen, M. Guina, T. Südmeyer, G. Huber, and C. Kränkel, Opt. Lett. **39**, 6939 (2014).
6. R. Kariyama, H. Tanaka, K. Iijima, K. Hirosawa, and F. Kannari, in *European Conference on Lasers and Electro-Optics* (Optical Society of America, 2015), paper CA_P_23.
7. Q. Bao, H. Zhang, Y. Wang, Z. Ni, Y. Yan, Z. X. Shen, K. P. Loh, and D. Y. Tang, Adv. Funct. Mater. **19**, 3077 (2009).
8. Z. Qin, G. Xie, C. Zhao, S. Wen, P. Yuan, and L. Qian, Opt. Lett. **41**, 56 (2016).
9. U. Keller, Nature **424**, 831 (2003).
10. R. Zhang, Y. Zhang, H. Yu, H. Zhang, R. Yang, B. Yang, Z. Liu, and J. Wang, Adv. Opt. Mater. **3**, 1787 (2015).
11. S. Lu, L. Miao, Z. Guo, X. Qi, C. Zhao, H. Zhang, S. Wen, D. Tang, and D. Fan, Opt. Express **23**, 11183 (2015).
12. J. Beránek, M. Hugenschmidt, U. Keller, G. Marowsky, G. Marowsky, K. Rohlena, W. Schulz, W. Seelig, P. Simon, U. Sowada, S. Szatmári, J. Uhlenbusch, W. Viöl, and R. Wester, *Laser Physics and Applications* (Springer, 2007).
13. K. S. Novoselov, A. K. Geim, S. V. Morozov, D. Jiang, Y. Zhang, S. V. Dubonos, I. V. Grigorieva, and A. A. Firsov, Science **306**, 666 (2004).
14. S. Wang, H. Yu, H. Zhang, A. Wang, M. Zhao, Y. Chen, L. Mei, and J. Wang, Adv. Mater. **26**, 3538 (2014).
15. K. F. Mak, C. Lee, J. Hone, J. Shan, and T. F. Heinz, Phys. Rev. Lett. **105**, 136805 (2010).
16. H. Zhang, S. Lu, J. Zheng, J. Du, S. Wen, D. Tang, and K. Loh, Opt. Express **22**, 7249 (2014).
17. Z. Tian, K. Wu, L. Kong, N. Yang, Y. Wang, R. Chen, W. Hu, J. Xu, and Y. Tang, Laser Phys. Lett. **12**, 065104 (2015).
18. H. J. Conley, B. Wang, J. I. Ziegler, R. F. Haglund, Jr., S. T. Pantelides, and K. I. Bolotin, Nano Lett. **13**, 3626 (2013).
19. Q. Liu, L. Li, Y. Li, Z. Gao, Z. Chen, and J. Lu, J. Phys. Chem. C **116**, 21556 (2012).
20. Y. Zhang, S. Wang, H. Yu, H. Zhang, Y. Chen, L. Mei, A. Di Lieto, M. Tonelli, and J. Wang, Sci. Rep. **5**, 11342 (2015).
21. G. Zhao, S. Han, A. Wang, Y. Wu, M. Zhao, Z. Wang, and X. Hao, Adv. Funct. Mater. **25**, 5292 (2015).
22. N. Kumar, S. Najmaei, Q. Cui, F. Ceballos, P. M. Ajayan, J. Lou, and H. Zhao, Phys. Rev. B **87**, 161403 (2013).
23. H. Li, Q. Zhang, C. C. R. Yap, B. K. Tay, T. H. T. Edwin, A. Olivier, and D. Baillargeat, Adv. Funct. Mater. **22**, 1385 (2012).
24. E. Garmire, IEEE J. Sel. Top. Quantum Electron. **6**, 1094 (2000).
25. K. Wang, J. Wang, J. Fan, M. Lotya, A. O'Neill, D. Fox, Y. Feng, X. Zhang, B. Jiang, and Q. Zhao, ACS Nano **7**, 9260 (2013).
26. H. Haus, IEEE J. Sel. Top. Quantum Electron. **12**, 169 (1976).
27. C. Hönninger, R. Paschotta, F. Morier-Genoud, M. Moser, and U. Keller, J. Opt. Soc. Am. B **16**, 46 (1999).
28. F. Cornacchia, A. Di Lieto, M. Tonelli, A. Richter, E. Heumann, and G. Huber, Opt. Express **16**, 15932 (2008).